



Permeability of the porcine iris stroma

Royston K.Y. Tan^a, Xiaofei Wang^{a,b}, Anita S.Y. Chan^{c,d}, Monisha Esther Nongpiur^c, Craig Boote^{a,e}, Shamira A. Perera^{c,d}, Michaël J.A. Girard^{a,c,*}

^a Ophthalmic Engineering & Innovation Laboratory, Department of Biomedical Engineering, Faculty of Engineering, National University of Singapore, Singapore

^b Beijing Advanced Innovation Center for Biomedical Engineering, School of Biological Science and Medical Engineering, Beihang University, Beijing, China

^c Singapore Eye Research Institute, Singapore National Eye Centre, Singapore

^d Duke-NUS Medical School, Singapore

^e Structural Biophysics Group, School of Optometry and Vision Sciences, Cardiff University, UK

ARTICLE INFO

Keywords:

Hydraulic permeability
Iris biomechanics
Biphasic tissue
Angle closure glaucoma
Aqueous humor
Iris pigment epithelium
Dilator muscles
Sphincter muscles

ABSTRACT

Current literature has not considered or provided any data on the permeability of the iris stroma. In this study, we aimed to determine the hydraulic permeability of porcine irides from the isolated stroma. Fifteen enucleated porcine eyes were acquired from the local abattoir. The iris pigment epithelium was scraped off using a pair of forceps and the dilator muscles were pinched off using a pair of colibri toothed forceps. We designed an experimental setup, based on Darcy's law, and consisting of a custom 3D-printed pressure column using acrylonitrile butadiene styrene (ABS) plastic. PBS solution was passed through the iris stroma in a 180° arc shape, with a column height of approximately 204 mm (2000 Pa). Measurements of iris stromal thickness were conducted using optical coherence tomography (OCT). To measure flow rate, we measured the mass (volume) of PBS solution using a mass balance in approximately 1 min. Histology was performed using hematoxylin and eosin (H & E) and anti-smooth muscle antibody (anti- α -SMA) for validation. The permeability experiments demonstrated that the iris stroma is a biphasic tissue that allows fluid flow. Our image processing results determined the area of flow to be 7.55 mm² and the tissue thickness to be between 180 and 430 μ m. The hydraulic permeability of the porcine stroma, calculated using Darcy's law, was $5.13 \pm 2.39 \times 10^{-5}$ mm²/Pa·s. Histological and immunochemical studies confirmed that the tissues used for this permeability study were solely iris stroma. Additionally, anti- α -SMA staining revealed staining specific for stromal blood vessels, with the notable absence of dilator and sphincter muscle staining. Our study combined experimental microscopic data with the theory of biphasic materials to investigate the hydraulic permeability of the iris stroma. This work will serve as a basis on which to validate future biomechanical studies of human irides with which may ultimately aid disease diagnosis and inform the design of novel treatments.

1. Introduction

Over several decades, the biomechanics of a number of ocular tissues have been extensively researched, notably the cornea (Elsheikh et al., 2007; Kotecha et al., 2006; Nguyen and Boyce, 2011; Woo et al., 1972), sclera (Girard et al., 2009; Norman et al., 2011; Woo et al., 1972) and optic nerve head (Anderson, 1969; Sigal et al., 2004, 2005; Zhang et al., 2017). A key motivation of investigating the properties of these tissues is to predict or correlate changes in biomechanics to the susceptibility and progress of ocular diseases, such as glaucoma (Coudrillier et al., 2012; Norman et al., 2011) and myopia (McBrien et al., 2009; Shen et al., 2008). While most of these tissues have been

explored in depth, their complexities are commonly simplified in experimental and computational studies. An example is the iris tissue, which is composed of both solid and fluid components (Fredde, 1996; Gregersen, 1961), although commonly modelled using incompressible solid biomechanical models. Accordingly, further characterization of the iris' mechanical properties will facilitate improved computational models that could be used to further our understanding of existing pathologies.

The anterior segment of the eye constantly experiences movement of aqueous humor (Fredde, 1996; Gregersen, 1961; Kaufman et al., 2011), which is secreted by the ciliary body and drained through the trabecular meshwork (Kaufman et al., 2011; Mark, 2003; Pant and

* Corresponding author. Ophthalmic Engineering & Innovation Laboratory, Department of Biomedical Engineering, National University of Singapore, Engineering Block 4, #04-08, 4 Engineering Drive 3, 117583, Singapore.

E-mail address: mgirard@nus.edu.sg (M.J.A. Girard).

<https://doi.org/10.1016/j.exer.2019.02.005>

Received 8 November 2018; Received in revised form 11 January 2019; Accepted 4 February 2019

Available online 07 February 2019

0014-4835/ © 2019 Elsevier Ltd. All rights reserved.

Amini, 2018; Wiederholt, 1998). During miosis and mydriasis, aqueous humor flows in and out of the iris tissue, rendering it not just a simple solid tissue, but a biphasic one that accommodates both the inflow and outflow of fluids. Anatomically, the iris stroma is composed of a sponge-like meshwork (Quigley, 2010), porous in the middle to allow fluid movements within the anterior volume. It is composed of fibroblasts and melanocytes that form a cellular matrix, along with vasculature, neural elements and a connective tissue extracellular matrix (Freddo, 1996). The iris margin and posterior surfaces are bounded by sphincter and dilator muscles and iris pigment epithelium (IPE). The IPE contain apicolateral junctional complexes composed of tight and adherens junctions that form a blood aqueous barrier to limit fluid migrating posteriorly (Freddo, 1996; Mark, 2003). As such, the permeable stroma and non-permeable IPE should be delineated as separate tissues for a more accurate representation of the iris in computational modelling.

Current literature is limited in representing the biomechanical properties of irides by using incompressible solid models. Simple linear elastic models (Heys and Barocas, 1999) had previously been used, which are insufficient to accurately model organic tissues. More complex non-linear elastic models such as neo-Hookean (Whitcomb et al., 2009) and second order Ogden models (Zhang et al., 2014) are better in reflecting soft tissues (Ogden et al., 2004), but are still lacking in complexity due to the assumption of an incompressible solid tissue. Jouzdani used both a compressible and an incompressible neo-Hookean model in an attempt to model the stress-strain data (Jouzdani, 2013). To improve on existing models, we had previously utilized an isotropic elastic model for the solid phase of the biphasic stroma as well as the second order Ogden model to reflect the non-linearity of both the sphincter and dilator muscles (Tan et al., 2018). However, no current literature considered or provided any data on the hydraulic permeability of the iris stroma. In this study, we aimed to: (1) isolate the stroma from porcine irides, and to (2) perform flow experiments to determine the hydraulic permeability of porcine irides from the isolated stroma.

2. Material and methods

2.1. Sample preparation

Fifteen enucleated porcine eyes were purchased from a local porcine abattoir. (Singapore Food Industries Pte Ltd., Singapore). The fresh porcine eyes were transported back to the laboratory where experiments were completed within 36 h post mortem.

To isolate the iris stroma, the posterior iris tissues needed to be removed. Each isolated iris tissue was first immersed in phosphate buffer solution (Phosphate buffered saline tablets, Sigma-Aldrich, Missouri) and the iris pigment epithelium was scraped off using a pair of forceps (Heiss jewelers forceps #3C). Since only a small portion of the iris tissue was required for the experiment, each isolated iris tissue was split into two. Half of the tissue had the dilator muscle removed whereas the other half had not. The latter was processed with histology for validation purposes.

Next, using a pair of colibri toothed forceps (0.12 mm), the dilator muscles were slowly pinched off, small areas at a time. Since the dilator muscles' orientation is radial, it was crucial to gently peel them off across this direction. During this process, it was possible that small amounts of stroma tissue might have been removed. Priority was given to limiting the amount of dilator muscle tissue remaining while preventing any holes in the iris stroma that could affect its permeability. After removal of the dilator muscles, visual confirmation was done using an inverted microscope (Olympus IX51 & IX71, Olympus Corporation, Tokyo, Japan) (Fig. 1).

2.2. Permeability experiment using Darcy's law

The Navier-Stokes equation (Chorin, 1968; Temam, 2001) describes

motion of fluid substances and can be used to determine the permeability of the iris stroma. Homogenization of the Navier-Stokes equation will yield Darcy's law (Keller, 1980; Whitaker, 1986):

$$Q = \frac{\kappa A \Delta P}{\mu \Delta x} \text{ (mm}^3/\text{ s)} \quad (1)$$

Where the Q is the flow rate (mm³/s), κ is the permeability (mm²), A is the surface area of flow (mm²), ΔP is the pressure difference across the tissue (Pa), μ is the dynamic viscosity of the fluid (Pa·s) and Δx is the thickness of the tissue (mm). We defined our parameter to be the hydraulic permeability, used in similar biphasic biological tissue experimentation such as the meniscus (Périer et al., 2005). It is defined by the permeability of the tissue divided by the viscosity of the fluid, which is the PBS solution in our experiment:

$$\text{Hydraulic Permeability} = \frac{\kappa}{\mu} = \frac{Q \Delta x}{A \Delta P} \text{ (mm}^2/\text{ Pa}\cdot\text{s)} \quad (2)$$

Using Darcy's law, it was possible to obtain the hydraulic permeability of the iris stroma by setting a specific pressure difference and measuring the resulting flow rate. We designed an experimental setup consisting of a custom 3D-printed pressure column using acrylonitrile butadiene styrene (ABS) plastic (Fig. 2A). The stroma was positioned within the device such that it fully blocked the channel opening with no gap or leakage. The isolated iris tissue was then clamped using two nuts and bolts between the ABS plastic (Fig. 2B). The height of the pressure column was approximately 204 mm to provide a pressure difference across the iris stroma tissue of 2000 Pa (= 15 mmHg). The PBS level was maintained constant manually. The fluid flowed through the channel (crescent-shaped; arc-width: 1.1 mm; total area: 7.55 mm²) and through the stroma above the removed dilator muscle (Fig. 2C). The device was then clamped tight around the stroma. The experiment was conducted in the laboratory under a controlled room temperature of 24.0 °C. To estimate the flow rate, we measured the mass (and volume) of PBS solution at the channel output in under 1 min using a mass balance (Precisa XT220A, Precisa Gravimetrics AG, Dietikon, Switzerland; accuracy: 0.1 mg).

To validate that PBS was flowing only through the iris stroma, the prior isolated tissues with intact dilator muscles were also tested following the exact same protocol. We observed insignificant flow, suggesting that: 1) the dilator muscles are impermeable (Gregersen, 1961); and that 2) the setup was stable with no leakages, and the flow rate measured in the prior experiment was purely through the iris stroma.

2.3. Measuring iris stroma thickness

Each iris stroma sample had varying thickness that needed to be measured. We placed the iris tissue samples on a glass slide and used optical coherence tomography (OCT) to obtain images. The images were processed using Matlab (Version, 2015a; Mathworks, Inc., Natick, MA, USA). During the permeability experiment, only a small crescent-shaped portion of the iris stroma was subjected to a pressure gradient. We positioned the tissue in the center of the experimental setup to ensure that our estimated thickness of the stroma was in the same location. We were able to visually inspect and select the relevant OCT slices and iris stroma area for the thickness measurements. Each OCT image had a resolution of 10.84 μm/pixel, with an area of 100 × 100 pixels manually isolated for measurement (1.084 mm arc width measured) (Fig. 3A). Using Matlab, we processed the images to obtain the number of pixels corresponding to the tissue and obtained the average thickness for that slice (Fig. 3B). For each sample, 3 OCT images were selected and processed to obtain the average thickness.

2.4. Validation of parameters, histology and immunochemistry

We performed histology to validate that the tissues used in the experiment were indeed the iris stroma. Following the permeability

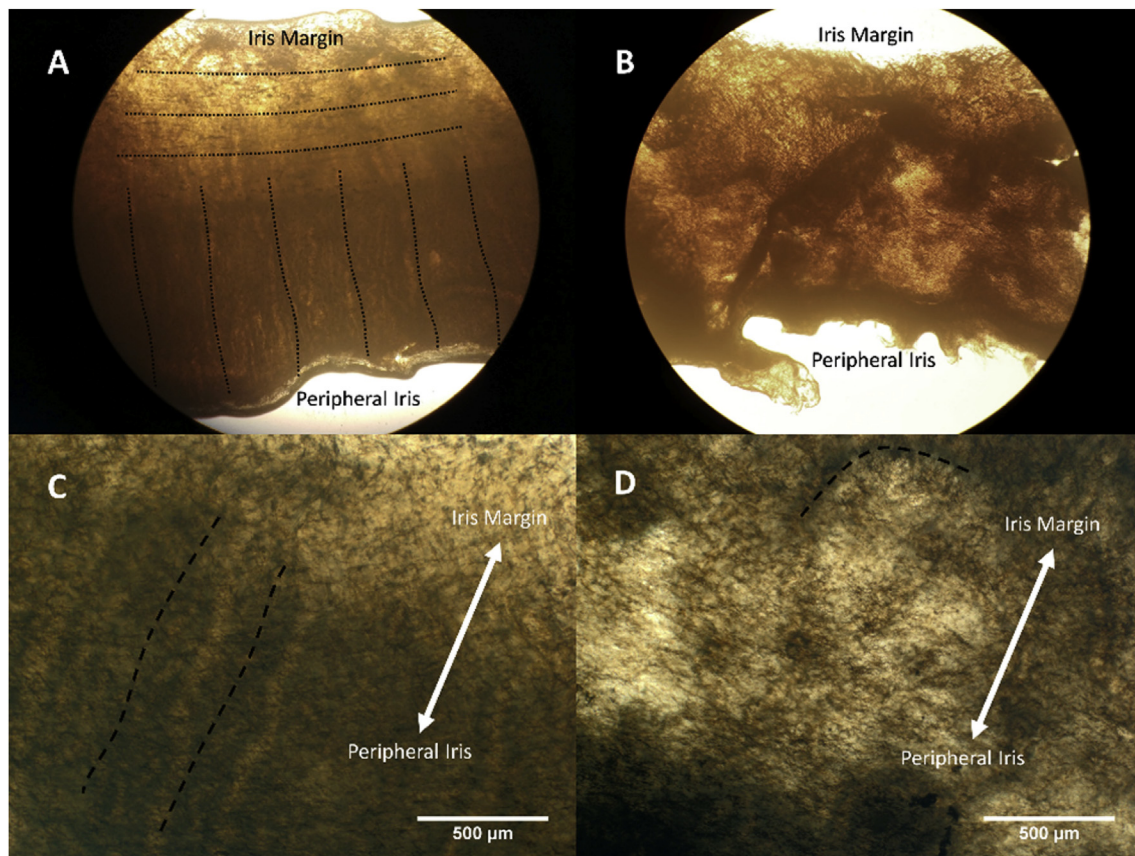


Fig. 1. Microscope images of the porcine iris using inverted microscopes. **(A)** Iris before posterior tissue removal. The iris margin is represented at the top of the image, and the periphery represented at the bottom. The sphincter and dilator muscles' locations are represented by the three black arc lines and six black wavy lines respectively. **(B)** Iris after posterior tissue removal. The dilator muscles were visibly absent compared to the image from **A**. **(C)** $4\times$ magnification of the iris before posterior tissue removal. The dilator muscles were clearly visible in the direction indicated by the two black wavy lines. **(D)** $4\times$ magnification of the iris after posterior tissue removal. Although most of the dilator tissues had been removed, priority was given to prevent any potential tears. Small amounts of posterior tissues may remain, indicated by the curved black line.

experiment, samples with and without dilator muscles were immersion fixed in 10% neutral buffered formalin solution for 24 h. These specimens were processed (Leica Surgipath, Leica Biosystems Richmond, Inc.) at the Ophthalmic Pathology Service, Singapore National Eye Centre, processed and then embedded in paraffin according to established protocols (Hollows and Graham, 1966). Using previously described histological techniques (Wang et al., 2018), deparaffinised $4\ \mu\text{m}$ thick sections were stained with hematoxylin and eosin (H&E) using an autostainer (Leica Autostainer XL; Leica Instrument, Nussloch, Germany), and then coverslipped. Immunohistochemistry was also performed with anti-alpha smooth muscle antibody (anti- α -SMA) (Abcam ab5694, 1:200 dilution with alkaline phosphatase chromogen) using our previously described protocol (Chan et al., 2017).

3. Results

The permeability experiment demonstrated that the iris stroma is a biphasic tissue that allows fluid flow. Without removal of the posterior tissues, the experimental setup observed insignificant flow. This confirmed that vertical column fluid pressure of approximately 2000 Pa caused fluid to flow directly through the tissue, without external factors such as leakage.

Image processing measured the area of flow to be $7.55\ \text{mm}^2$. The thickness of each tissue was evaluated using OCT and image processing and found to be between 180 and $430\ \mu\text{m}$. The variance in thickness was due to anatomical differences and varying difficulties in isolating the iris stroma. As expected, samples that had greater thickness demonstrated less flow, since these variables are typically inversely

proportional.

We were able to calculate the hydraulic permeability of each tissue sample using Darcy's law. The hydraulic permeability of the porcine stroma was $5.13 \pm 2.39 \times 10^{-5}\ \text{mm}^2/\text{Pa}\cdot\text{s}$, with a total of 15 samples evaluated.

Histological and immunochemical experiments confirmed that the tissues used for this permeability study were solely iris stroma. The iris pigment epithelium (IPE) is visible as a dark brown pigment under the microscope (Fig. 4A and B). For our samples, the IPE was clearly absent (Fig. 4C). Anti- α -SMA staining revealed stroma blood vessels, sphincter and dilator muscles, visible as red stains under the microscope. Our immunochemical study revealed that, after sample preparation, the sphincter and dilator muscles were successfully removed, as evidenced by the absence of the red stain (Fig. 4D).

4. Discussion

In this study, we performed an *ex vivo* experiment to investigate the hydraulic permeability value of porcine irides and validated our methods using histology. We found that our method of posterior iris tissue removal was effective in isolating only the iris stroma for the experiment. We were able to obtain a hydraulic permeability value of $5.13 \pm 2.39 \times 10^{-5}\ \text{mm}^2/\text{Pa}\cdot\text{s}$, which had not been investigated in the current literature. This could potentially be crucial for disease diagnosis because changes in iris biomechanical properties, specifically permeability, could be correlated to disease development.

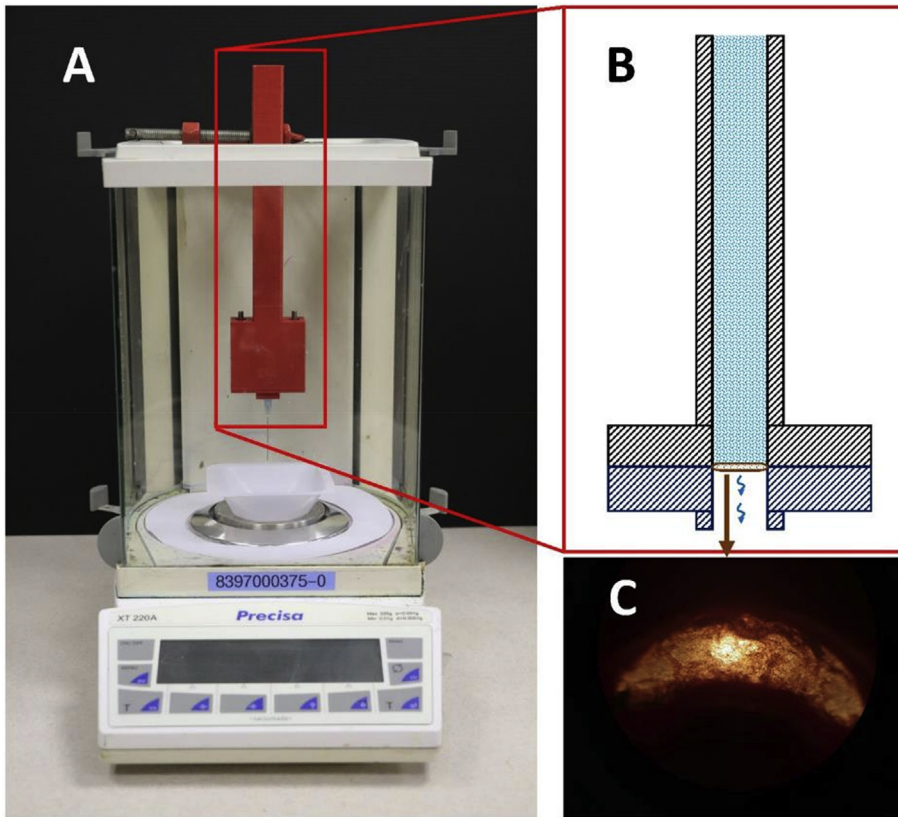


Fig. 2. Permeability experiment setup. (A) The 3D printed column is secured on a mass balance to measure the amount of flow. (B) The column secured a sample of the iris stroma and vertical pressure causes the PBS solution to flow through the tissue. (C) The area of flow had a curved rectangular shape to account for the circular shape of the iris tissue.

4.1. A highly permeable iris stroma allows for effective ocular physiology

An iris stroma that is highly permeable to aqueous humor is essential for physiological ocular functions. Miosis and mydriasis occur rapidly at a rate of approximately 4 mm/s (Morgan et al., 1968). During these processes, the two iris muscles contract and relax antagonistically to constrict or dilate the pupil, resulting in increase or decrease of iris volume, respectively. This is facilitated by the high permeability of the iris stroma, allowing for rapid movement of aqueous humor in and out of the iris (Freddo, 1996; Gregersen, 1961; Hoper et al., 1989; Kinsey et al., 1955; Mark, 2003), such that pupil accommodation can be achieved quickly. In contrast, the human meniscus has a hydraulic permeability of $1.99 \pm 0.79 \times 10^{-9} \text{ mm}^2/\text{Pa}\cdot\text{s}$ (Joshi et al., 1995) for slow exudation of fluid out of the tissue, in order to balance the loads on the articular bone surfaces.

The high permeability of the iris stroma is also essential to delivery of oxygen and nutrients to the surrounding ocular tissues (Freddo, 1996; Hoper et al., 1989; Kinsey et al., 1955). Movement of aqueous humor, produced in the iris and outflow through the trabecular meshwork (Goel et al., 2010), along with processes such as buoyancy-driven flow, miosis and mydriasis, phacodonesis, etc., contribute to the effective distribution of nutrients to tissues in the anterior chamber (Fitt and Gonzalez, 2006; Freddo et al., 1990; Goel et al., 2010). As such, loss of permeability of the iris stroma could disrupt aqueous flow and physiological functions, potentially leading to the development of ocular diseases.

4.2. Permeability of the iris stroma could be directly related to pathologies

In diseases such as primary angle closure glaucoma (PACG), the

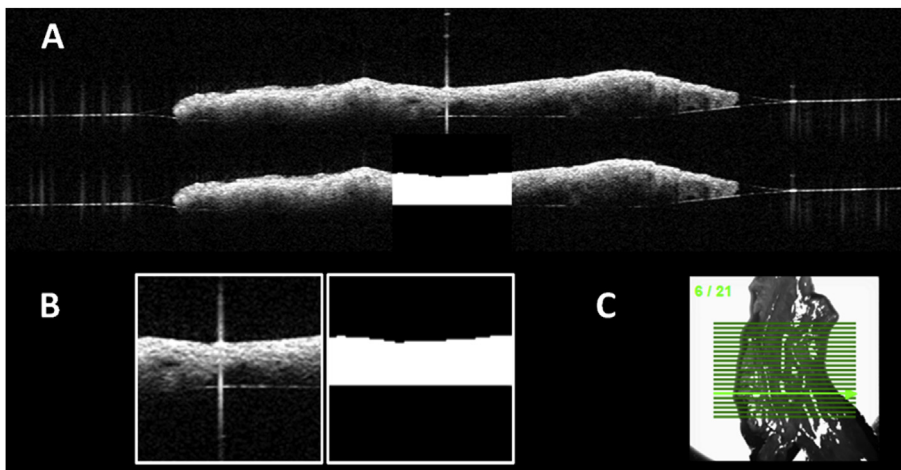


Fig. 3. OCT images were taken and processed to investigate the porcine iris stroma thickness. (A) The raw OCT image (above) was processed to identify the boundaries of the tissue (below). An area of 100×100 pixels that was used for the experiment was isolated manually by inspecting the top view of the slice and selecting the center portion for analysis. (B) Matlab was used to process the image, to ensure the image was orientated horizontally and the appropriate pixels were used for measurement. Filters, alignment and thresholding was utilized to obtain a clean image. (C) A total of 3 images were processed per tissue sample and the average was taken for calculation.

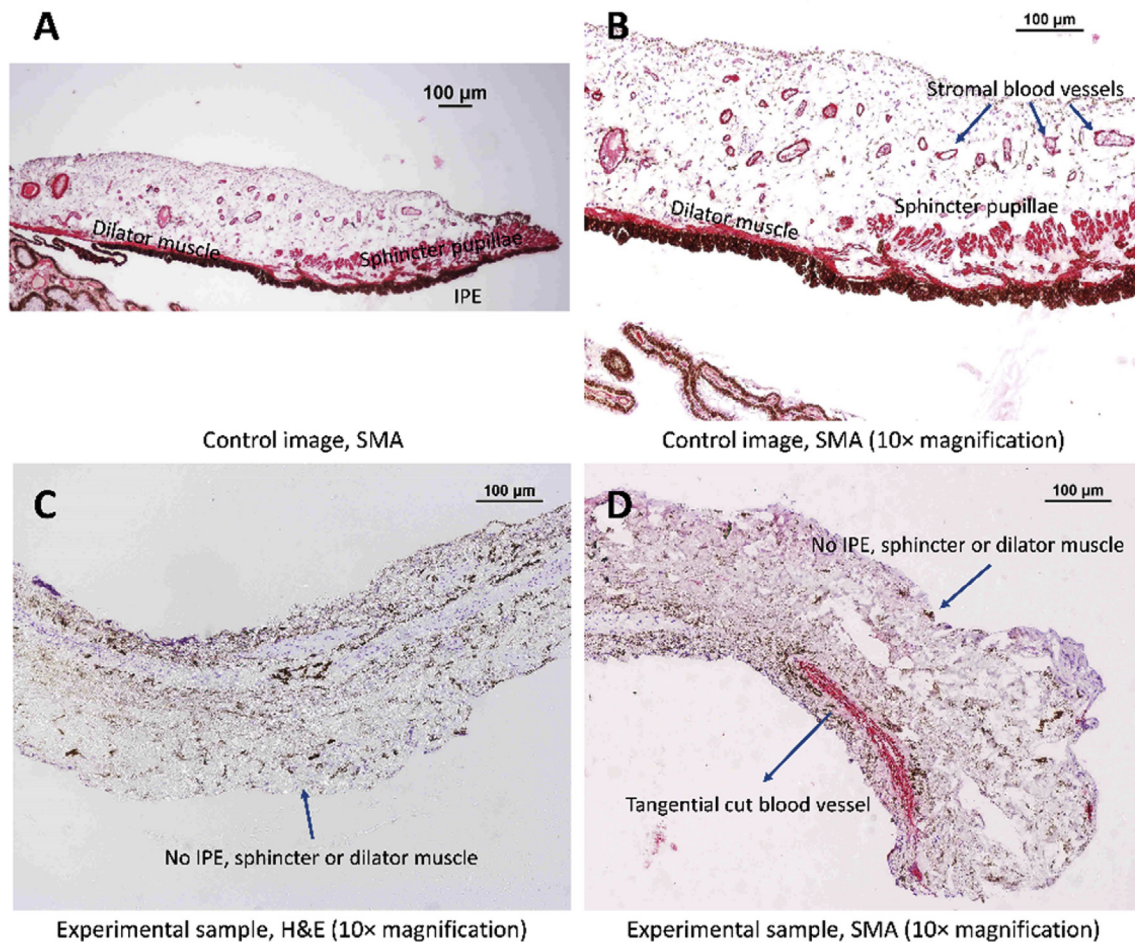


Fig. 4. Histology and immunohistochemistry of the iris tissue. (A) A control image of the porcine iris tissue composed of stroma and iris pigment epithelium, stained with anti- α -SMA to highlight the iris sphincter muscle, iris dilator muscle and perivascular smooth muscles. (B) 10 \times magnification of the porcine iris tissue stained with anti- α -SMA shows an intact IPE with positive red staining (red chromagen, SMA, Abcam) of the muscles within the iris. (C) 10 \times magnification of a porcine tissue sample used for the permeability experiment, stained with H&E. In contrast to the control images, the heavily pigmented iris pigment epithelium (IPE) is absent, together with the sphincter and dilator muscles. (D) 10 \times magnification of a porcine tissue sample used for the permeability experiment, stained with anti- α -SMA and with hematoxylin counter-stain. The positive perivascular smooth muscle smooth muscle staining serves as an positive internal control, and confirms the absence of both iris sphincter and dilator muscles at the posterior iris border.

irides behave differently compared to those in healthy subjects or those with primary open angle glaucoma (POAG). During mydriasis and miosis, the change in tissue permeability could be crucial for early detection of PACG. Some studies found that in PACG, there was less volume change during mydriasis (Aptel and Denis, 2010; Quigley et al., 2009; Tun et al., 2014). This caused the iris to bulge significantly at the periphery, closing the angle and blocking aqueous flow out of the anterior chamber. Notably, for the Asian population with brown irides, a naturally shallower anterior chamber creates a more acute drainage angle that could increase the incidence of PACG. Interestingly, other studies reported more volume change during mydriasis (Mak et al., 2013), or potentially none for certain subtypes of PACG (Narayanaswamy et al., 2013). It is possible that the apparently conflicting findings of these research studies could be reconciled by investigating the permeability of the iris tissue. By improving FE models to account for the biphasic properties of the iris stroma, inverse FE modelling could be performed to obtain these parameters and correlate them to PACG.

Angle closure eyes also demonstrate distinct iris surface features including darker colour with fewer iris crypts compared to eyes with wider angles (Sidhartha et al., 2014). Iris crypts are described as regions of iris stroma hypoplasia or atrophy. The presence of a greater number of crypts is suggestive of a more porous iris stroma which allows a

better flow of aqueous across the iris. It is also speculated that higher melanocyte and melanin content in darker irides contribute to a greater iris stromal thickness, making it less permeable to aqueous.

Interestingly, PLEKHA7, a gene associated with PACG (Vithana et al., 2012) and which encodes an apical junctional protein that is expressed in components of the blood aqueous barrier (BAB) (Lee et al., 2014), was found to be down-regulated in iris tissue of PACG patients (Lee et al., 2017). BAB includes the tight junctions of the non-pigmented ciliary epithelium (NPCE), the iris capillary endothelial cells and the posterior iris epithelium. It is suggested that alterations in PLEKHA7 occurring in PACG may result in compromised barrier changes, the consequences of which can be dysregulated paracellular fluid movement that may contribute to the etiology of PACG. Additionally, the dynamic increase in iris volume with pupil dilation (Aptel and Denis, 2010; Quigley et al., 2009) in PACG may be attributed to a reduction in PLEKHA7, which causes alterations in structural integrity of cellular junctions and results in aberrant permeability at the level of the iris vascular endothelium or iris pigment epithelium (Lee et al., 2017). Furthermore, the slower speed of pupil constriction in eyes with angle closure (Zheng et al., 2012) may be ascribed to variations in iris permeability.

4.3. The iris tissue could be better represented with more accurate finite element (FE) models

The biomechanical properties of the iris are important because deviations from physiological behaviour of this tissue had been observed in diseases such as angle closure glaucoma (Aptel and Denis, 2010; Pant et al., 2018; Quigley et al., 2009). Prior biomechanical studies omitted the permeability of the iris stroma, instead obtaining the moduli of the iris tissues as a whole (Heys and Barocas, 1999; Jouzdani, 2013; Lei et al., 2008; Whitcomb et al., 2009, 2011; Zhang et al., 2014). It is therefore likely that the higher collagen content in PACG eyes compared to POAG, may render it more rigid and impact tissue permeability (Chua et al., 2008; He et al., 2008; Seet et al., 2016). Therefore, in computational studies, a simplified iris tissue model had always been utilized. By investigating the permeability of the iris stroma tissue, we emphasize the need for more accurate computational models that better reflect the behaviour of these tissues.

Previously, we had incorporated the biphasic properties of the iris tissue to create a more biofidelic FE model (Tan et al., 2018). This model allowed for changes in iris tissue volume during miosis and mydriasis, observed in volume and cross-sectional area calculations from OCT images. With the adoption of a more representative FE model, we will be able to study how changes in iris tissue biomechanical properties could relate to various ocular diseases.

4.4. Limitations

The current study was subject to several limitations. First, during tissue sample preparation there were remnants of the posterior tissues remaining. Since these tissues are far stiffer than the delicate anterior stroma, it was likely that any attempt to remove all the posterior tissues would result in tearing and these holes would invalidate the permeability test. Priority was given to maintaining the integrity and uniformity of the iris stroma and, thus, some of the flow could have been blocked at regions with incomplete tissue removal, reducing the measured permeability of that sample.

Second, due to the long preparation time required, each tissue was tested within 36 h post-mortem, during which the structural properties of the iris stroma could have changed. Specifically, the fibroblasts, melanocytes and nerve cells could have lost cell integrity after death (Kanduc et al., 2002). Since they make up most of the stroma matrix, a loss of structural integrity could have increased the permeability of the tissue.

Third, the exit flow could have been affected by slight negative pressures caused by accumulation of large water droplets. These large water droplets could have extended several millimetres downwards, creating pressures of up to -50 Pa. We attached a needle to drain and maintain a steady outflow of PBS, avoiding excessive accumulation of fluid at the mouth of the setup. This would reduce the effect of the negative pressure to a negligible amount.

Fourth, the pressure column could have induced slight compression of the tissue, affecting the iris thickness measurements. This could have led to smaller hydraulic permeability values calculated from a more compact tissue. In fact, during miosis and mydriasis, the arrangement and tissue density of the iris stroma would differ, creating a range of permeability values. In this study, we focused our measurements on the iris stroma during miosis, where the permeability of the tissue is greater.

Finally, our experimental setup required manual refill of PBS solution as it flowed through the tissue. Even though the flow of fluid is slow, there was still a small variation of pressure as the fluid column decreased and increased. We limited the variation of pressure to within ± 2 mm ($< 1\%$ of 2000 Pa). Therefore, the results of the experiment should not have been significantly affected by this issue.

5. Conclusion

Our study combined experimental microscopic data on the iris tissue with the theory of poroelastic materials to investigate the permeability of the iris stroma. This work may serve as a basis on which to validate future biomechanical studies of human irides, which may ultimately aid in the diagnosis of diseases such as PACG, and could help to inform the design of novel ocular treatments.

Funding

This work was supported by funding from the SNEC-HREF Device R & D fund (R1412/98/2016).

References

- Anderson, D.R., 1969. Ultrastructure of human and monkey lamina cribrosa and optic nerve head. *Arch. Ophthalmol.* 82, 800–814.
- Aptel, F., Denis, P., 2010. Optical coherence tomography quantitative analysis of iris volume changes after pharmacologic mydriasis. *Ophthalmology* 117, 3–10.
- Chan, A.S., Mudhar, H., Shen, S.Y., Lang, S.S., Fernando, M., Hilmy, M.H., Guppy, N.J., Rennie, I., Dunkley, L., Al Jajeh, I., 2017. Serum IgG2 and tissue IgG2 plasma cell elevation in orbital IgG4-related disease (IgG4-RD): potential use in IgG4-RD assessment. *Br. J. Ophthalmol.* 101, 1576–1582.
- Chorin, A.J., 1968. Numerical solution of the Navier-Stokes equations. *Math. Comput.* 22, 745–762.
- Chua, J., Seet, L.F., Jiang, Y., Su, R., Htoon, H.M., Charlton, A., Aung, T., Wong, T.T., 2008. Increased SPARC expression in primary angle closure glaucoma iris. *Mol. Vis.* 14, 1886.
- Coudrillier, B., Tian, J., Alexander, S., Myers, K.M., Quigley, H.A., Nguyen, T.D., 2012. Biomechanics of the human posterior sclera: age-and glaucoma-related changes measured using inflation testing. *Investig. Ophthalmol. Vis. Sci.* 53, 1714–1728.
- Elsheikh, A., Wang, D., Brown, M., Rama, P., Campanelli, M., Pye, D., 2007. Assessment of corneal biomechanical properties and their variation with age. *Curr. Eye Res.* 32, 11–19.
- Fitt, A., Gonzalez, G., 2006. Fluid mechanics of the human eye: aqueous humour flow in the anterior chamber. *Bull. Math. Biol.* 68, 53.
- Freddo, T.F., 1996. Ultrastructure of the iris. *Microsc. Res. Tech.* 33, 369–389.
- Freddo, T.F., Bartels, S., Barsotti, M., Kamm, R.D., 1990. The source of proteins in the aqueous humor of the normal rabbit. *Investig. Ophthalmol. Vis. Sci.* 31, 125–137.
- Girard, M.J., Downs, J.C., Bottlang, M., Burgoyne, C.F., Suh, J.-K.F., 2009. Peripapillary and posterior scleral mechanics—part II: experimental and inverse finite element characterization. *J. Biomech. Eng.* 131, 051012.
- Goel, M., Picciani, R.G., Lee, R.K., Bhattacharya, S.K., 2010. Aqueous humor dynamics: a review. *Open Ophthalmol. J.* 4, 52.
- Gregersen, E., 1961. On the imbibition of the human Iris stroma with the aqueous humour: summary of thesis. *Acta Ophthalmol.* 39, 623–625.
- He, M., Lu, Y., Liu, X., Ye, T., Foster, P.J., 2008. Histologic changes of the iris in the development of angle closure in Chinese eyes. *J. Glaucoma* 17, 386–392.
- Heys, J., Barocas, V., 1999. Mechanical characterization of the bovine iris. *J. Biomech.* 32, 999–1003.
- Hollows, F., Graham, P., 1966. Intra-ocular pressure, glaucoma, and glaucoma suspects in a defined population. *Br. J. Ophthalmol.* 50, 570.
- Hoper, J., Funk, R., Zagorski, Z., Rohen, J., 1989. Oxygen delivery to the anterior chamber of the eye—a novel function of the anterior iris surface. *Curr. Eye Res.* 8, 649–659.
- Joshi, M.D., Suh, J.K., Marui, T., Woo, S.L.Y., 1995. Interspecies variation of compressive biomechanical properties of the meniscus. *J. Biomed. Mater. Res.* 29, 823–828.
- Jouzdani, S., 2013. Biomechanical Characterization and Computational Modeling of the Anterior Eye. University Of Minnesota.
- Kanduc, D., Mittelman, A., Serpico, R., Sinigaglia, E., Sinha, A.A., Natale, C., Santacroce, R., Di Corcia, M.G., Lucchese, A., Dini, L., 2002. Cell death: apoptosis versus necrosis. *Int. J. Oncol.* 21, 165–170.
- Kaufman, P.L., Adler, F.H., Levin, L.A., Alm, A., 2011. *Adler's Physiology of the Eye*. Elsevier Health Sciences.
- Keller, J.B., 1980. Darcy's law for flow in porous media and the two-space method. *Nonlinear Partial Differ. Equ. Eng. Appl. Sci.* 31, 429–443.
- Kinsey, V.E., Palm, E., Cavanaugh, G.A., 1955. Posterior and anterior chamber aqueous humor formation. *AMA Arch. Ophthalmol.* 53, 330–344.
- Kotecha, A., Elsheikh, A., Roberts, C.R., Zhu, H., Garway-Heath, D.F., 2006. Corneal thickness-and age-related biomechanical properties of the cornea measured with the ocular response analyzer. *Investig. Ophthalmol. Vis. Sci.* 47, 5337–5347.
- Lee, M.-C., Shei, W., Chan, A.S., Chua, B.-T., Goh, S.-R., Chong, Y.-F., Hilmy, M.H., Nongpiur, M.E., Baskaran, M., Khor, C.-C., 2017. Primary angle closure glaucoma (PACG) susceptibility gene PLEKHA7 encodes a novel Rac 1/Cdc42 GAP that modulates cell migration and blood-aqueous barrier function. *Hum. Mol. Genet.* 26, 4011–4027.
- Lee, M.C., Chan, A.S.Y., Goh, S.R., Hilmy, M.H., Hong, W., Aung, T., Hunziker, W., Vithana, E.N., 2014. Expression of primary angle closure glaucoma (PACG) susceptibility gene PLEKHA7 in cells of the blood aqueous barrier. *Investig. Ophthalmol. Vis. Sci.* 55 5718–5718.

- Lei, Y., Zhang, K., Chen, C., Song, H., Li, T., Lin, D., Liu, Z., 2008. Experimental research on the mechanical properties of porcine iris. *Clin. Biomech.* 23, S83–S87.
- Mak, H., Xu, G., Leung, C.K.-S., 2013. Imaging the iris with swept-source optical coherence tomography: relationship between iris volume and primary angle closure. *Ophthalmology* 120, 2517–2524.
- Mark, H.H., 2003. Aqueous humor dynamics and the iris. *Med. Hypotheses* 60, 305–308.
- McBrien, N.A., Jobling, A.L., Gentle, A., 2009. Biomechanics of the sclera in myopia: extracellular and cellular factors. *Optom. Vis. Sci.* 86, E23–E30.
- Morgan, S.S., Hollenhorst, R.W., Ogle, K.N., 1968. Speed of pupillary light response following topical pilocarpine or tropicamide. *Am. J. Ophthalmol.* 66, 835–844.
- Narayanaswamy, A., Zheng, C., Perera, S.A., Htoon, H.M., Friedman, D.S., Tun, T.A., He, M., Baskaran, M., Aung, T., 2013. Variations in iris volume with physiologic myopia in subtypes of primary angle closure glaucoma. *Investig. Ophthalmol. Vis. Sci.* 54, 708–713.
- Nguyen, T., Boyce, B., 2011. An inverse finite element method for determining the anisotropic properties of the cornea. *Biomechanics Model. Mechanobiol.* 10, 323–337.
- Norman, R.E., Flanagan, J.G., Sigal, I.A., Rausch, S.M., Tertinegg, I., Ethier, C.R., 2011. Finite element modeling of the human sclera: influence on optic nerve head biomechanics and connections with glaucoma. *Exp. Eye Res.* 93, 4–12.
- Ogden, R., Saccomandi, G., Sgura, I., 2004. Fitting hyperelastic models to experimental data. *Comput. Mech.* 34, 484–502.
- Pant, A.D., Amini, R., 2018. 19. Iris biomechanics. *Biomechanics of the Eye* 281.
- Pant, A.D., Gogte, P., Pathak-Ray, V., Dorairaj, S.K., Amini, R., 2018. Increased iris stiffness in patients with a history of angle-closure glaucoma: an image-based inverse modeling analysis. *Investig. Ophthalmol. Vis. Sci.* 59, 4134–4142.
- Périé, D., Korda, D., Iatridis, J.C., 2005. Confined compression experiments on bovine nucleus pulposus and annulus fibrosus: sensitivity of the experiment in the determination of compressive modulus and hydraulic permeability. *J. Biomech.* 38, 2164–2171.
- Quigley, H.A., 2010. The iris is a sponge: a cause of angle closure. *Ophthalmology* 117, 1–2.
- Quigley, H.A., Silver, D.M., Friedman, D.S., He, M., Plyler, R.J., Eberhart, C.G., Jampel, H.D., Ramulu, P., 2009. Iris cross-sectional area decreases with pupil dilation and its dynamic behavior is a risk factor in angle closure. *J. Glaucoma* 18, 173–179.
- Seet, L.F., Narayanaswamy, A., Finger, S.N., Htoon, H.M., Nongpiur, M.E., Toh, L.Z., Ho, H., Perera, S.A., Wong, T.T., 2016. Distinct iris gene expression profiles of primary angle closure glaucoma and primary open angle glaucoma and their interaction with ocular biometric parameters. *Clin. Exp. Ophthalmol.* 44, 684–692.
- Shen, M., Fan, F., Xue, A., Wang, J., Zhou, X., Lu, F., 2008. Biomechanical properties of the cornea in high myopia. *Vis. Res.* 48, 2167–2171.
- Sidhartha, E., Nongpiur, M.E., Cheung, C.Y., He, M., Wong, T.Y., Aung, T., Cheng, C.-Y., 2014. Relationship between iris surface features and angle width in Asian eyes. *Investig. Ophthalmol. Vis. Sci.* 55, 8144–8148.
- Sigal, I.A., Flanagan, J.G., Ethier, C.R., 2005. Factors influencing optic nerve head biomechanics. *Investig. Ophthalmol. Vis. Sci.* 46, 4189–4199.
- Sigal, I.A., Flanagan, J.G., Tertinegg, I., Ethier, C.R., 2004. Finite element modeling of optic nerve head biomechanics. *Investig. Ophthalmol. Vis. Sci.* 45, 4378–4387.
- Tan, R.K., Wang, X., Perera, S.A., Girard, M.J., 2018. Numerical stress analysis of the iris tissue induced by pupil expansion: comparison of commercial devices. *PLoS One* 13, e0194141.
- Temam, R., 2001. Navier-Stokes Equations: Theory and Numerical Analysis. American Mathematical Soc.
- Tun, T.A., Baskaran, M., Perera, S.A., Chan, A.S., Cheng, C.-Y., Htoon, H.M., Sakata, L.M., Cheung, C.Y., Aung, T., 2014. Sectoral variations of iridocorneal angle width and iris volume in Chinese Singaporeans: a swept-source optical coherence tomography study. *Graefes Arch. Clin. Exp. Ophthalmol.* 252, 1127–1132.
- Vithana, E.N., Khor, C.-C., Qiao, C., Nongpiur, M.E., George, R., Chen, L.-J., Do, T., Abu-Amero, K., Huang, C.K., Low, S., 2012. Genome-wide association analyses identify three new susceptibility loci for primary angle closure glaucoma. *Nat. Genet.* 44, 1142.
- Wang, X., Teoh, C.K.G., Chan, A.S., Thangarajoo, S., Jonas, J.B., Girard, M.J., 2018. Biomechanical properties of bruch's membrane–choroid complex and their influence on optic nerve head biomechanics. *Investig. Ophthalmol. Vis. Sci.* 59, 2808–2817.
- Whitaker, S., 1986. Flow in porous media I: a theoretical derivation of Darcy's law. *Transport Porous Media* 1, 3–25.
- Whitcomb, J.E., Amini, R., Simha, N.K., Barocas, V.H., 2011. Anterior–posterior asymmetry in iris mechanics measured by indentation. *Exp. Eye Res.* 93, 475–481.
- Whitcomb, J.E., Barnett, V.A., Olsen, T.W., Barocas, V.H., 2009. Ex vivo porcine iris stiffening due to drug stimulation. *Exp. Eye Res.* 89, 456–461.
- Wiederholt, M., 1998. Direct involvement of trabecular meshwork in the regulation of aqueous humor outflow. *Curr. Opin. Ophthalmol.* 9, 46–49.
- Woo, S.-Y., Kobayashi, A., Schlegel, W., Lawrence, C., 1972. Nonlinear material properties of intact cornea and sclera. *Exp. Eye Res.* 14, 29–39.
- Zhang, K., Qian, X., Mei, X., Liu, Z., 2014. An inverse method to determine the mechanical properties of the iris in vivo. *Biomed. Eng. Online* 13, 1.
- Zhang, L., Thakku, S.G., Beotra, M.R., Baskaran, M., Aung, T., Goh, J.C., Strouthidis, N.G., Girard, M.J., 2017. Verification of a virtual fields method to extract the mechanical properties of human optic nerve head tissues in vivo. *Biomechanics Model. Mechanobiol.* 16, 871–887.
- Zheng, C., Cheung, C.Y., Narayanaswamy, A., Ong, S.-H., Perera, S.A., Baskaran, M., Chew, P.T., Friedman, D.S., Aung, T., 2012. Pupil dynamics in Chinese subjects with angle closure. *Graefes Arch. Clin. Exp. Ophthalmol.* 250, 1353–1359.